Optimizing the biofabrication process of omentum-based scaffolds for engineering autologous tissues

2014 Biofabrication 6 035023

(http://iopscience.iop.org/1758-5090/6/3/035023)

IOP Publishing Biofabrication

Biofabrication 6 (2014) 035023 (14pp) doi:10.1088/1758-5082/6/3/035023

Optimizing the biofabrication process of omentum-based scaffolds for engineering autologous tissues

Neta Soffer-Tsur[1,2], Michal Shevach[1,3], Assaf Shapira[1], Dan Peer[2,3,4] and Tal Dvir[1,3,4]

[1] The laboratory for tissue engineering and regenerative medicine, Department of Molecular microbiology and Biotechnology, George S. Wise Faculty of Life Science, Tel Aviv University, Tel Aviv 69978, Israel
[2] The laboratory of nanomedicine, Department of Cell Research and Immunology, George S. Wise Faculty of Life Sciences, Tel Aviv University, Tel Aviv 69978, Israel
[3] The Center for Nanoscience and Nanotechnology, Tel Aviv University, Tel Aviv 69978, Israel
[4] Department of Materials Science and Engineering, Tel Aviv University, Tel Aviv 69978, Israel

E-mail: tdvir@post.tau.ac.il

Received 2 February 2014, revised 11 June 2014
Accepted for publication 22 July 2014
Published 27 August 2014

Abstract

Omentum-based matrices fabricated by decellularization have the potential to serve as autologous scaffolds for tissue engineering. Transplantation of such scaffolds prepared from the patient's own biomaterial may reduce the immunogenic response after transplantation. Recently we reported on the potential of the decellularized omentum to support the assembly of functional vascularized cardiac patches. Here we compared five distinct protocols for omentum decellularization, utilizing chemical, physical and biological processes. We analyzed the efficiency of cell removal, scaffold macro and micro structure, biochemical composition and the ability of seeded cells to attach and proliferate in the matrix. Moreover, we assessed the ability of the distinct scaffolds to promote the organization of cardiac tissue.

Keywords: cardiac tissue engineering, decellularization, omentum, scaffolds

(Some figures may appear in colour only in the online journal)

Introduction

Organ transplantation holds the only hope of survival for many individuals and promises the only possibility of a good quality of life for many others [1]. Unfortunately the number of organs available for transplantation is far exceeded by the number of patients in the waiting list [2, 3]. Cellular therapies rely on the basis of the concept that when isolated cells are injected to the defected organ they can restore, maintain or improve tissue function [4]. However, several drawbacks may jeopardize the success of this approach, namely the lack of control at the cell accumulation site and cell death by apoptosis due to lack of cell–cell or cell–matrix interactions [5–7].

In vivo, cells are supported by the extracellular matrix (ECM), a self-assembled three-dimensional (3D) network of biomolecules, which provides the cells with a wealth of physical and biochemical signals inducing tissue structure and function [8–12]. In tissue engineering, one of the goals is to synthetically design 3D biomaterials that closely mimic the ECM and support the cells until they secrete their own matrix proteins. However, the detailed structure and composition of the natural matrix, which fosters such cellular organization, are still not well understood and therefore it is extremely complicated to precisely summarize the process [13–15].

In recent years, many groups have used decellularized matrices as scaffolds for engineering functional tissues, including heart valves, blood vessels, urinary bladders and heart muscles [16–20]. In this approach tissues and organs are usually harvested from animals and the cells are removed by chemical, physical and biological techniques [13]. Thus the underlying matrix, including most of the essential biomolecules such as collagen fibers and glycosaminoglycans (GAGs), is preserved. After cell seeding, the obtained

Table 1. Graphic description of the five distinct protocols for omentum decellularization.

Step	*Protocol#1*	*Protocol#2*	*Protocol#3*	*Protocol#4*	*Protocol#5*
Hypotonic shock	10mM tris + 5mM EDTA + 1uM PMSF pH 8.0 – 1h	10mM tris + 5mM EDTA + 1uM PMSF pH 8.0 – 1h	10mM tris + 5mM EDTA + 1uM PMSF pH 8.0 – 1h X2 and overnight	10mM tris + 5mM EDTA + 1uM PMSF pH 8.0 – 1h X2 and overnight	X
Freeze - thaw	In hypotonic buffer, -80*C to 37*C X3	In hypotonic buffer, -20*C to -80*C to 37*C	X	X	X
Dehydration	70% ethanol 100% ethanol X3	70% ethanol 100%ethanol X3	70% ethanol 100% ethanol X3	70% ethanol 100% ethanol X3	70% ethanol 100% ethanol X3
Fat extraction	Acetone X3 40:60 **acetone: hexane** – 24 h	Isopropanol X3 40:60 **isopropanol: hexane** – 24h	**Acetone** – 24h	**Acetone** – 24h	Acetone X3 **50:50 acetone: hexane** **20:80 acetone: hexane** – 24h
Rehydration	100% ethanol 70% ethanol	100% ethanol 70% ethanol	100% ethanol 70% ethanol	100% ethanol 70% ethanol	100% ethanol 70% ethanol
Cell extraction	**Trypsin** – overnight at RT	**Trypsin** 1h at 37*C 50mM tris+ 1mM MgCl2+ 1% Triton pH8.0 – 1h	10mM tris + 5mM EDTA – 2h 1% **SDS** in ddw – 24h 2.5mM **Sodium deoxycholate** in PBS – 2h X2 ***	10mM tris + 5mM EDTA – 2h 1% **SDS** in ddw – 24h 2.5mM **Sodium deoxycholate** in PBS – 2h X2	50mM tris + 1% MgCl2 + 1% triton pH7.4 – 30 min
Nucleic degradation	50mM tris + 1mM MgCl2 pH8.0 – 30 min 50mM tris + 1mM MgCl2 + 0.1% BSA + 40U/ml **benzonase** – 20h at 37*C	50mM tris + 1mM MgCl2 pH8.0 – 30 min X2 50mM tris + 1mM MgCl2 + 0.1% BSA + 40U/ml **benzonase** – 20h at 37*C	50mM tris + 1mM MgCl2 pH8.0 – 30 min 50mM tris + 1mM MgCl2 + 0.1% BSA + 40U/ml **benzonase** – 20h at 37*C	50mM tris + 1mM MgCl2 pH8.0 – 30 min 50mM tris + 1mM MgCl2 + 0.1% BSA + 40U/ml **benzonase** – 20h at 37*C	50mM tris + 1% MgCl2 + 1% triton pH7.4 + 41.8U/ml **benzonase** – 20h
Continuing cell extraction and washing	50mM tris + 1% triton – 1h 50mM tris PBS X3 Ddw X3	50mM tris + 1% triton – 1h 50mM tris PBS X3 Ddw X3	50mM tris + 1% triton – 1h 50mM tris PBS X3 Ddw X3	50mM tris + 1% triton – 1h 50mM tris * Second fat extraction step: • Dehydration • Acetone X3 • **40:60 acetone: hexane –** 24h • Rehydration PBS X3 Ddw X3	50mM tris + 5mM MgCl2 + 1% triton pH7.4 – 2h X2 1M NaCl + 20mM EDTA+ 0.2% triton pH 7.0 – 1h Ddw X4
Lyophilization	Freezing at -20*C Lyophilizing	Freezing at -20*C Lyophilizing	Freezing at -20*C Lyophilizing	Freezing at -20*C Lyophilizing	X

*** **Protocols#3-4**: Repeat fat and cell extraction steps

xenogeneic scaffolds can support the growth of the engineered tissue [21].

Recently, we reported on the fabrication of an omentum based 3D decellularized matrix for the engineering of cardiac tissue [22]. The omentum is highly vascularized adipose tissue that extends from the stomach overlying the abdomen [23]. The regenerative properties of the omentum have long been demonstrated [24, 25]. Here, we have optimized the decellularization process of the omentum. We have tested 5 distinct protocols for cell and fat extraction from the tissue and characterized the obtained scaffolds in terms of efficiency of cell removal, macro and micro structure and biochemical content. Moreover, we have investigated the potential of the obtained scaffolds to maintain cell viability and support tissue growth.

Materials and methods

All materials were purchased from Sigma (Rehovot, IL) unless stated otherwise.

Decellularization

Two different omenta of healthy pigs were purchased from the institute of animal research in Kibutz Lahav, Israel. The fresh tissues were washed with phosphate buffered saline (PBS) in order to deplete blood and debris. Each organ was then cut into five 30–50 g pieces. Each piece from each pig was treated with a different protocol for decellularization. Overall, every decellularization protocol was conducted on two different omenta. After weighing the decellularized tissues, the samples were kept frozen for further analysis. All steps of incubation and wash were obtained at room temperature on an orbital shaker unless noted otherwise. A summary of the distinct protocols appears in table 1.

*Protocol#*1. Fresh omentum was agitated for 1 h in a hypotonic buffer of 10 mM Tris 5 mM Ethylenediaminetetraacetic acid (EDTA) and 1 μM phenylmethanesulfonylfluoride (PMSF) at pH 8.0. Next, the tissue went through three cycles of freezing (−80 °C) and thawing (37 °C) using the same buffer. After the last thawing the tissue was dehydrated by washing it once with 70% ethanol for 30 min and three times in 100% ethanol for 30 min each. Then the polar lipids of the tissue were extracted by three 30 min washes of 100% acetone. Finely the apolar lipids were extracted by 24 h incubation in a 60/40 (v/v) hexane:acetone solution (with 3 changes). The defatted tissue was rehydrated by one 30 min wash in 100% ethanol and overnight incubation in 70% ethanol at 4 °C. Then the tissue was washed four times with PBS at pH 7.4 and was incubated in 0.25% Trypsin–EDTA (Biological Industries, Kibbutz Beit-Haemek, Israel) solution overnight. The tissue was then washed thoroughly with PBS and then with 50 mM Tris buffer with 1 mM $MgCl_2$ at pH 8.0 for 30 min Following this, the tissue was gently agitated in a nucleic degradation solution of 50 mM Tris, 1 mM $MgCl_2$, 0.1% bovine serum albumin (BSA) and 40 units/mL Benzonase® nuclease (Novagen, Madison, WI) at pH 8.0 for 20 h at 37 °C. Finally the tissue was washed with 50 mM Tris 1% triton-X100 solution at pH8.0 for 1 h. The decellularized tissue was washed once with 50 mM Tris at pH 8.0, three times with PBS and three times with double distilled water. The decellularized tissue was frozen (−20 °C) and lyophilized.

*Protocol #*2. Fresh omentum was agitated for 1 h in a hypotonic buffer of 10 mM Tris 5 mM EDTA and 1 μM PMSF at pH 8.0. Then the tissue went through one cycle of freezing (−80 °C) and thawing (37 °C) using the same buffer. The tissue was dehydrated by washing it once with 70% ethanol for 30 min and three times in 100% ethanol for 30 min each. Then the polar lipids of the tissue were extracted by three 30 min washes of 100% isopropanol. Finely the apolar lipids were extracted by 24 h incubation in a 60/40 (v/v) hexane:isopropanol solution (with three changes). The defatted tissue was rehydrated by one 30 min wash in 100% ethanol and overnight incubation in 70% ethanol at 4 °C. Then the tissue was washed four times with PBS at pH 7.4 and incubated in 0.25% Trypsin–EDTA solution for 1 h at 37 °C. The tissue was then washed thoroughly with PBS and then with 50 mM Tris buffer with 1 mM $MgCl_2$ and 1% triton-X100 at pH 8.0 for 1 h. The tissue was washed twice in a 50 mM Tris-1 mM $MgCl_2$ at pH 8.0 for 30 min each. Then the tissue was gently agitated in a nucleic degradation solution of 50 mM Tris 1 mM $MgCl_2$ 0.1% BSA and 40 units/mL Benzonase® nuclease at pH 8.0 for 20 h at 37 °C. Finally the tissue was washed with 50 mM Tris 1% triton-X100 solution at pH 8.0 for 1 h. The decellularized tissue was washed once with 50 mM Tris at pH 8.0, three times with PBS and three times with double distilled water. The decellularized tissue was frozen (−20 °C) and lyophilized.

*Protocol #*3. Fresh omentum was agitated for 24 h in a hypotonic buffer of 10 mM Tris 5 mM EDTA and 1 μM PMSF at pH8.0 (with 3 changes). The tissue was dehydrated by washing it once with 70% ethanol for 30 min and 3 washes of 100% ethanol for 30 min each. Then the tissue was incubated for 24 h in 100% acetone (with 3 changes) for lipid extraction. The tissue was rehydrated with one 30 min wash in 100% ethanol and overnight incubation in 70% ethanol at 4 °C. Then the tissue was washed four times with PBS at pH 7.4 and then incubated for 2 h in the hypotonic solution. The tissue was further processed with 1% sodium dodecyl sulphate (SDS) solution for 24 h (with 2 changes) following two 2 h incubations in 2.5 mM sodium deoxycholate in PBS. The tissue was dehydrated again, incubated for 24 h in 100% acetone and rehydrated. Then the tissue was treated again with the hypotonic buffer for 2 h followed by 24 h in 1% SDS and two 2 h incubations in 2.5 mM sodium deoxycholate. The tissue was then washed thoroughly with PBS and then with 50 mM Tris-1 mM $MgCl_2$ at pH 8.0 for 1 h. The tissue was gently agitated in a nucleic degradation solution of 50 mM Tris 1 mM $MgCl_2$ 0.1% BSA and 40 units/mL Benzonase® nuclease at pH 8.0 for 20 h at 37 °C. Finally the tissue was washed twice with 50 mM Tris at pH 8.0 (1 h each), three times with PBS and three times with double distilled water. The decellularized tissue was frozen (−20 °C) and lyophilized.

Protocol #4. Fresh omentum was first treated exactly as in protocol #3, only with one cycle of fat extraction with 100% acetone. After the nucleic degradation step the tissue was dehydrated by washing it once with 70% ethanol for 30 min and 3 washes of 100% ethanol for 30 min each. Following, the tissue was washed 3 times in 100% acetone. Finely the apolar lipids were extracted by 24 h incubation in a 60/40 (v/v) hexane:acetone solution (with 3 changes). The defatted tissue was rehydrated by one 30 min wash in 100% ethanol and 30 min wash in 70% ethanol at 4 °C. The processed tissue was then washed three times with PBS and three times with double distilled water. The decellularized tissue was frozen (−20 °C) and lyophilized.

Protocol #5. Fresh omentum was dehydrated by washing it once with 70% ethanol for 30 min and three washes of 100% ethanol for 30 min each. Then the tissue was washed three times with 100% acetone for 1 h and once with 50/50 (v/v) acetone:hexane solution. The tissue was incubated for 24 h in 20/80 (v/v) acetone:hexane solution (with three changes) for lipid extraction. The tissue was rehydrated by one 30 min wash in 100% ethanol and overnight incubation in 70% ethanol at 4 °C. The defatted tissue was washed with 50 mM Tris buffer with 1 mM $MgCl_2$ and 1% triton-X100 at pH 7.4 for 30 min and then was incubated for 20 h in a fresh solution that contains 40 units/mL Benzonase® nuclease. Next the tissue was washed twice with 50 mM Tris 5 mM $MgCl_2$ and 1% Triton-X100 at pH 7.4 for 2 h, and then for 1 h in 1 M NaCl 20 mM EDTA and 0.2% Triton-X100 at pH7.0. Finally the tissue was washed with double distilled water and was stored in 70% ethanol at 4 °C.

Assessing lipids remains

Dried samples (20 mg) from the native tissue or from the decellularized matrices that were processed by each protocol were digested in 1 mL digestion solution containing 1.7 mg mL^{-1} papain for 4 h at 65 °C. The digested samples were centrifuged at 10 000 g for 5 min After centrifugation the lipids that remained in the digested tissues became visible as an upper phase.

DNA staining and quantification

For nucleic acid detection, small pieces from the native and the processed tissues were stained with 5 μg mL^{-1} Hoechst 33258 for 3 min followed by washes with PBS. The samples were visualized using an inverted fluorescence microscope (Nikon Eclipse TI).

DNA was extracted from three random dry samples (25–30 mg) of the native and decellularized tissues using DNeasy Blood & Tissue Kit (Qiagen, Hilden, Germany) according to the manual guide. The obtained DNA was quantified by measurements of the O.D at 260 nm wavelength using a spectrophotometer (Nanodrop 1000, Thermo Scientific).

Sulfated glycosaminoglycan quantification

The sulfated glycosaminoglycans (GAGs) in the native and processed tissues were quantified using the Blyscan sulfated GAG assay kit (Biocolor Ltd, Carrickfergus, UK) according to the manufacturer instructions. Briefly, the tissues were digested with papain. The digested solutions were centrifuged and the supernatants were examined with dimethylmethylene blue. Overall, four samples were used for each assay.

Histology

Samples from the native and the processed tissues (of the same animal) were fixed in formalin and embedded in paraffin. Sections of 5 μm were obtained and affixed to X-tra® adhesive glass slides (Leica Biosystems, Wetzler, Germany). The slides were stained with hematoxylin and eosin (H&E; Merck, Geneva, Switzerland) in order to confirm decellularization, and with Alcian-blue and Fast-red (Merck) for GAG imaging.

Scanning electron microscopy

For scanning electron microscopy (SEM) imaging, punches from each scaffold that contained both translucid and fatted areas were selected. Processed tissues from the same animal were fixed with 2.5% glutaraldehyde in 0.2 M phosphate buffer at pH 7.4 for 2 h. Then the tissues were dehydrated using a graded series of ethanol-water solutions (50%–100%). Finally the samples were critical point dried and sputter coated with gold and then observed under SEM (Jeol JSM840A). The properties of the fibers and pores from 5 different photos that contained both areas of each scaffold were measured with ImageJ program (NIH).

Fibroblasts viability assessment

In order to assess the biocompatibility of the processed tissues, scaffolds (8 mm in diameter) were obtained from each protocol for incubation with NIH-3T3 mouse fibroblasts that were manipulated to express the enhanced green fluorescent protein (EGFP). First, the scaffolds were sterilized by UV light for 2 h. Next, cells (10^5) were seeded on each scaffold in triplicates for each time point. Three hours after seeding, the scaffolds were washed once and then incubated in Dulbecco's modified Eagle's medium (DMEM; Biological Industries) supplemented with 10% (v/v) fetal bovine serum and 1% (v/v) solution of 10 000 units ml^{-1} penicillin and 10 mg ml^{-1} streptomycin (Biological industries) at 37 °C. The scaffolds were observed on days 2 and 8 using an inverted fluorescence microscope (Nikon Eclipse TI). The viability of the cells was measured using an XTT cell proliferation assay kit (Biological industries) according to the manufacturer's instructions. Briefly, the cells containing scaffolds were incubated with the XTT reagent for 20 h at 37 °C. The optical density of the medium was measured at 450 nm and 630 nm. All the scaffolds were the products of the same omentum.

Cardiomyocytes culture

The procedure for cell isolation employed in this study was approved by the Animal Care and Use Committee of Tel Aviv University, Israel,research authority L-11-053. Neonatal ventricle myocytes (taken from 1- to 3-day-old Sprague-Dawley rats) were isolated using 6–7 cycles of enzyme digestion, as previously described in [26]. Briefly, left ventricles were harvested and minced, and cells were isolated using enzymatic digestion with collagenase type II (95 U mL^{-1}; Worthington, Lakewood, NJ) and pancreatin (0.6 mg mL^{-1}) in DMEM. After each round of digestion cells were centrifuged (600 g, 4 °C, 5 min) and re-suspended in the culture medium composed of M-199 supplemented with 0.6 mM $CuSO_4 \cdot 5H_2O$, 0.5 mM $ZnSO_4 \cdot 7H_2O$, 1.5 mM vitamin B12, 500 U mL^{-1} penicillin (Biological Industries) and 100 mg ml^{-1} streptomycin (Biological Industries), and 0.5% (v/v) FBS. To enrich the cardiomyocytes population, cells were suspended in the culture medium with 5% FBS and pre-plated twice for 30 mins. Cell number and viability was determined by a hemocytometer and trypan blue exclusion assay. Cardiac cells ($5 \cdot 10^5$) were seeded onto 5 mm diameter scaffolds by adding 10 μl of the suspended cells, followed by a 40 min incubation period (37 °C, 5% CO_2). Following this, cell constructs were supplemented with the culture medium (with 5% FBS) for further incubation.

Immunostaining

Immunostaining was performed as previously described [26]. Cardiac cell constructs were fixed and permeabilized in 100% cold methanol for 10 min, washed three times in a DMEM-based buffer and then blocked for 1 h at room temperature in DMEM-based buffer containing 2% FBS, after which the samples were washed three times with PBS. The samples were then incubated with primary antibodies to detect α-sarcomeric actinin (1:750, Sigma), washed three times and incubated for 1 h with Alexa Fluor 647 conjugated goat anti-mouse antibody (1:500; Jackson, West Grove, PA, USA). For nuclei detection, the cells were incubated for 3 min with 5 μg ml^{-1} Hoechst 33258 and washed three times. Samples were visualized using an inverted fluorescence microscope (Nikon Eclipse TI). All the scaffolds were the products of the same omentum.

Statistical analysis

Statistical analysis data are presented as average ± standard error. Differences between the groups were assessed with a one way ANOVA followed by Tukey post hoc test. All analyses were performed using a GraphPad Prism version 5.00 for Windows (GraphPad Software). $P < 0.05$ was considered significant. NS denotes $P > 0.05$, * denotes $P < 0.05$, ** denotes $P < 0.01$, *** denotes $p < 0.001$.

Results and discussion

In order to obtain decellularized scaffolds which are suitable for engineering functional tissues, two main conditions must be kept. First, it is crucial that cells and DNA fragments are removed from the matrix to prevent both toxicity *in vitro* and any immune response after transplantation. The second goal is preservation of the essential biomolecules of the ECM, including collagen fibers, GAGs and adhesion proteins.

The omentum is a highly vascularized, double sheet of peritoneum that extends from the greater curvature of the stomach overlying most abdominal organs [23, 27]. It has a unique cellular and extracellular composition, containing adipocytes that are embedded in a well vascularized connective tissue and a translucent region that includes mesothelial cells and collagen [28].

After processing the tissue with five protocols, we sought to evaluate the effect of the different protocols on cell removal and ECM preservation (see table 1 and materials and methods).

Rationale

The five protocols were developed using previously described decellularization and tissue processing methods [17, 21, 29–33]. The first protocol was developed in order to maximize elimination of cellular components without considering the preservation of the ECM and therefore was the most aggressive. The protocol combined mechanical, physical, chemical and biological approaches for decellularization. Protocol 2 was designed to reduce the damages to the ECM obtained by protocol 1. It constituted the same steps of protocol 1, however several of the steps were less aggressive. For example, the trypsin digestion step was shorter and the fat extraction step was conducted with isopropanol which is less reactive than the acetone used in protocol 1. Protocols 3 and 4 were based mostly on detergent and osmotic pressure for decellularization in order to further reduce the damages to the ECM, and differ from each other by the fat extraction step. For the fat extraction step in protocol 4 we have added the use of the apolar solvent hexane in order to also dissolve the apolar lipids in the tissue, whereas on protocol 3 we have used only the polar solvent acetone. Finally, in protocol 5 the decellularization started with fat extraction that was followed by nucleic acids degradation and a short exposure to a hypertonic environment and ionic detergent that are meant to disrupt cellular membranes.

Macroscopic structure

The effect of the different protocols was immediately detected in a macroscopic view (figure 1). Protocol 1, which involved 3 cycles of freezing and thawing and a long protease digestion, led to the disruption of the omental macrostructure (figure 1(A)). Protocol 2 involved only one cycle of freezing and thawing and 1 h of protease digestion. As shown, this protocol resulted in a less disrupted macrostructure. Protocol 3 involved a longer hypotonic treatment and use of the

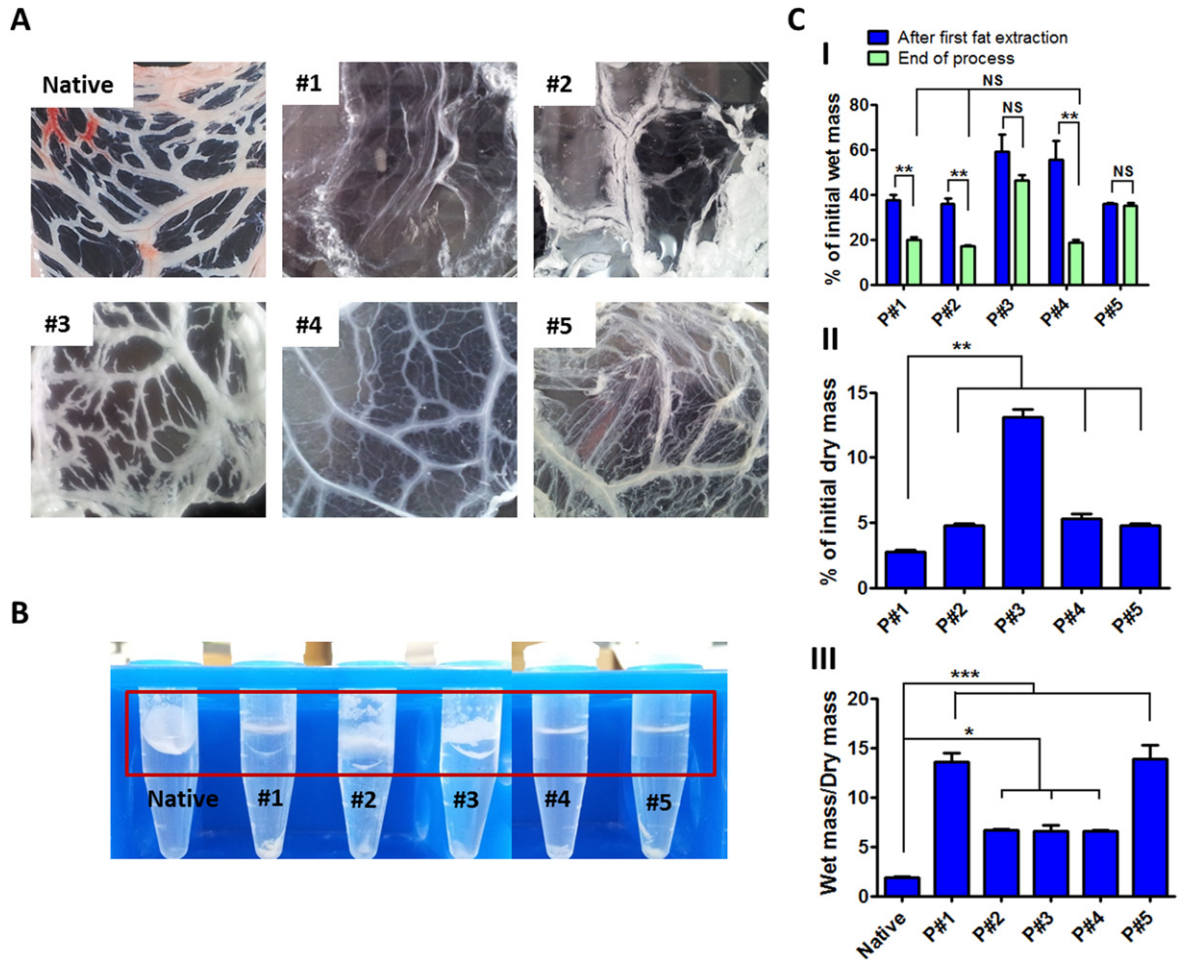

Figure 1. Decellularized matrices. A: Macroscopic images of the native omentum and the decellularized matrices obtained by the different protocols. B: A centrifuged digestion solution of 20 mg of each scaffold and the native tissue. The lipids that remained in the scaffolds are visible as an upper phase. C: Mass loss after decellularization. (I) Percentages of the wet remaining masses of the tissues during and after the decellularization processes. (II) Percentages of the remaining dry mass after decellularization. (III) The relation between the wet mass and the dry mass of the native and decellularized tissues at the end of the process, as an indication of the water absorbance property of the scaffolds.

anionic surfactant SDS which lyses cells. As shown in figure 1(A) the natural structure was conserved and the blood vessel infrastracture could be easily detected. However, fatty tissue could still be observed around the blood vessels. To efficiently remove the fat from the tissues we added hexane, an apolar solvent (protocol 4). As shown, the addition of this step resulted in better removal of the fatty tissue. The cell extraction steps in protocol 5 mainly relied on the use of the nonionic detergent triton X-100 and a short exposure to a hypertonic environment which causes cell lysis due to water flow out. The obtained structure resembled the structure of the native tissue. However, the yellow color of the tissue suggested the existence of cell components at the end of the process.

Lipid extraction

Another indication for the efficiency of fat extraction was the visual detection of lipids that are extracted from the tissues after enzymatic digestion (figure 1(B)). As shown in figure 1(B) a lipid phase was not detected in the tissues that were processed by protocols 1, 4 and 5. The omentum contains many adipocytes that are loaded with apolar lipids, such as triglycerides. Therefore, as expected, high lipid content was detected in the tissue that was processed by the polar solvent alone (protocol 3). Since the tissue was only treated with acetone for fat extraction the apolar lipids were not dissolved. Although a previously published paper has reported complete fat removal from the omentum by a polar solvent alone [34], our samples required the addition of an apolar solvent for fat elimination. Furthermore we have found a relatively high lipid content after treating the tissue with protocol 2, indicating that the combination of acetone and hexane (protocols 1, 4, 5) is more efficient than the use of isopropanol and hexane (protocol 2). That observation may be attributed to the fact that the ketone group in acetone is more reactive than the hydroxyl in isopropanol.

Mass reduction

We next sought to evaluate the efficiency of the decellularization process by tissue mass reduction. As shown in

figure 1(C)-I all decellularization protocols yielded a significant reduction in tissue mass, which occurred after the fat depletion step. Protocols 1, 2, and 5 combined the use of a polar solvent (i.e. acetone or isopropanol) with the apolar solvent hexane. The percentages of the remaining wet masses after the fat depletion step for those protocols were 37.4 ± 2.6, 35.8 ± 2.5 and 36.0 ± 0.32 of the initial mass, respectively. The first fat extraction step in protocol 3 and 4 was conducted with acetone only, therefore the apolar lipids did not dissolve and the remaining mass percentages were 58.9 ± 7.7 and 55.3 ± 8.7 respectively. The second fat extraction process in protocol 4 involved hexane and therefore resulted in an efficient extraction of the remaining lipids and a further 36.8% wet mass reduction from the initial mass. However, in protocol 3, the last decellularization steps (detergent treatments and nucleic digestion by nuclease) yielded only a 12.7% reduction in wet mass. In protocols 1, 2 and 4 the steps following the fat extraction yielded further significant mass reduction, indicating that more components were removed from the tissues. The lack of mass reduction in protocol 5 indicated that the processes that followed the fat extraction step (triton X-100 processing and a short hypertonic treatment) had minimal contribution to the decellularization process.

While investigating the dry masses of the processed tissues we have expected to obtain similar percentages of mass reduction compared with the wet mass loss. However, the dry mass assessments revealed that all protocols induced higher mass reduction than the observed wet mass loss. This phenomenon can be attributed to the increase in water absorbance of the processed tissues. The remaining wet masses after treating the tissues with protocols 1–5 were 19.83 ± 1.37, 16.91 ± 0.73, 46.19 ± 2.29, 18.5 ± 1.5 and 35.15 ± 1.22. However, as shown in figure 1(C)-II, the remaining dry masses after treating the tissues with protocols 1–5 were only $2.74\% \pm 0.19$, $4.75\% \pm 0.21$, $13.08\% \pm 0.649$, $5.28\% \pm 0.43$ and 4.74 ± 0.164 respectively. Interestingly, the results revealed that protocol 1 resulted in a higher dry mass reduction than protocols 2 and 4, although the wet mass reduction of these protocols was similar. That observation indicated that protocol 1 eliminated more components from the tissue, while resulting in a more water absorbing matrix.

The ratio between the wet mass and the dry mass of the scaffold indicated its ability to absorb water. As shown in figure 1(C)-III all protocols resulted in an increase of water absorbance compared with the native tissue, however a significantly higher absorption was found after treating the tissues with protocols 1 and 5. This can be attributed to a decrease in hydrophobic components such as lipids and an increase in the concentration of water absorbing ECM components, such as GAGs and collagens.

Cell removal

We next turned to evaluate the efficiency of cell and nucleic acid removal. The decellularized matrices were stained for nucleic acids by Hoechst 33258 or nuclei and cytoplasm by H&E (figures 2(A) and 3, respectively). Furthermore, the residual DNA in the matrices has been quantified (figure 2(B)). As shown in figure 2(A) a neglectable Hoechst staining was detected after processing the tissues with protocols 1, 3 and 4. Treating the tissues with protocols 2 and 5 resulted in no intact nuclei; however, the nucleic acids were not completely removed, indicating that the nucleases could not efficiently access the cells. As shown in figure 2(B), residual DNA quantification has revealed a significant reduction in DNA by all of the protocols (less than 100 ng DNA per mg dry tissue). Protocols 1–3 resulted in less than 50 ng DNA per mg dry tissue, which is considered as a completely decellularized scaffold [35]. Protocols 4 and 5 resulted in higher DNA content. Comparing the staining results of the scaffolds that were obtained by protocols 4 and 5 suggests that the remaining DNA was probably more degraded in protocol 4 than the DNA that remained with protocol 5, and therefore it could not be detected under the microscope.

Accordingly, H&E staining (figure 3) revealed the presence of cells and nuclei in the matrix processed by protocol 5, further supporting the assumption that the DNA was not efficiently degraded by that protocol. H&E staining of the matrices processed by protocols 1–4 revealed no cell debris.

The histological sections have also revealed differences in the morphologies of the processed tissues. The morphology of the native adipose tissue resembles a honeycomb structure due to the large adipocytes loaded with fat. In all of the processed tissues that underwent a fat extraction with apolar and polar solvents (i.e., protocols 1, 2, 4 and 5), the absence of lipids resulted in morphology changes. The fact that the structure of the matrix obtained by protocol 3 is still similar to that of the native tissue further supports the claim that a polar solvent alone is not sufficient for fat removal. Examination of the morphologies obtained by protocols 1, 2 and 4 revealed that protocol 1 was indeed more destructive to the ECM then protocol 2. This observation suggests that shorter trypsin digestion or less freezing and thawing cycles are less disruptive to the ECM. In addition, both protocols resulted in more ECM damage than protocol 4. This suggests that a treatment that includes freezing and thawing and trypsin digestion is more disruptive to the ECM than decellularization with tonicity and mild detergents.

GAG content

GAGs are long unbranched polysaccharides that are major components of the ECM. GAGs have numerous biological activities, namely they promote cell adhesion, control and regulate cell growth, and induce proliferation [36]. The high negative charge of the sulfated GAGs promotes electrostatic interactions with many growth factors and cytokines, providing their preservation and controlled release into the cellular microenvironment [12]. Therefore, the preservation of GAG content within the matrix may be beneficial for engineering complex tissues [13, 21]. To qualitatively assess GAG content at the end of the decellularization process, Alcian blue staining was used. Figure 4(A) revealed that all the treatments preserved GAGs to some extent, however

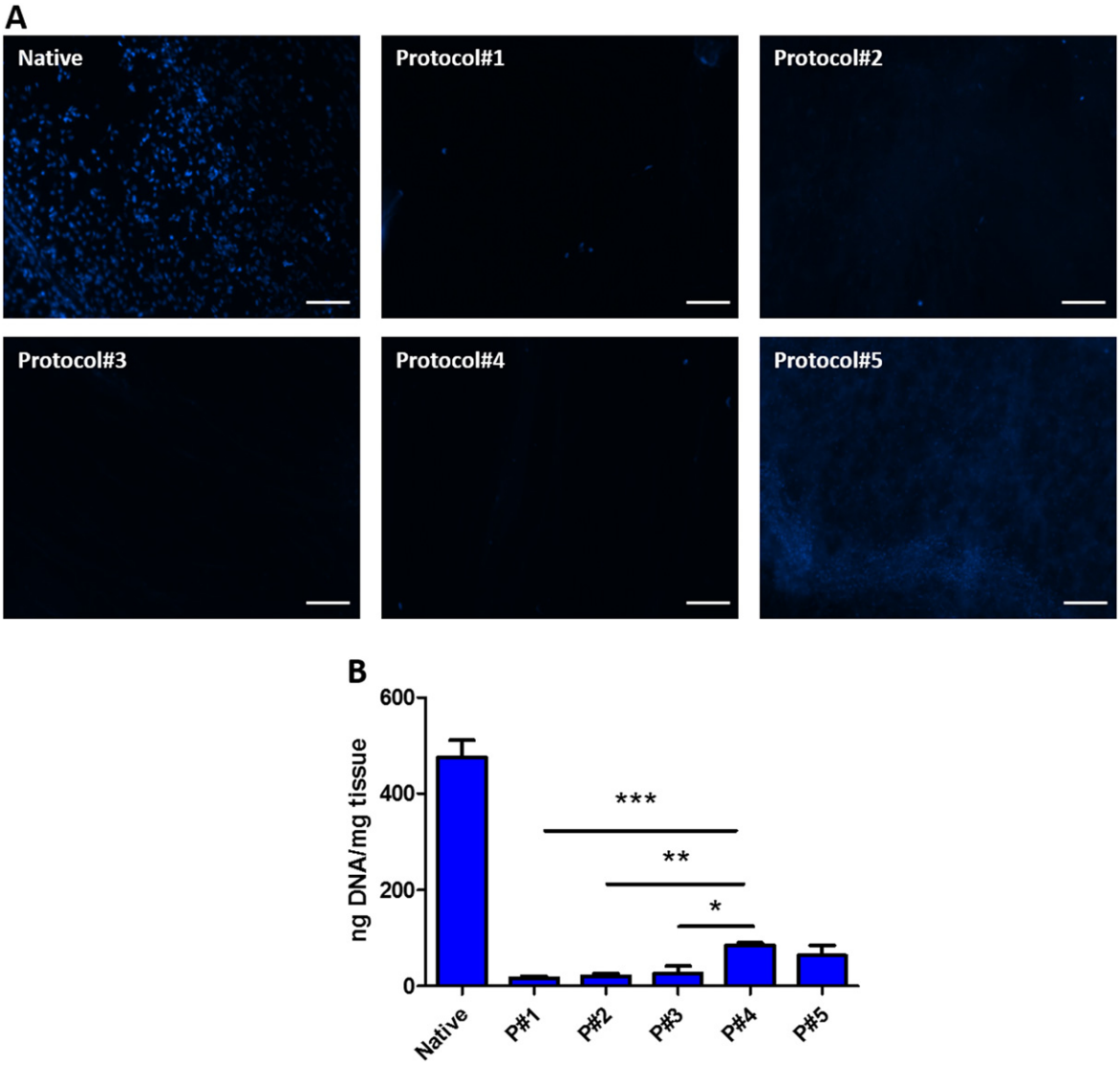

Figure 2. Nuclei elimination. A: Hoechst staining of the native tissue and the decellularized matrices obtained by the different protocols for the demonstration of the remaining DNA (scale bar = 100 μm). B: DNA quantification from 25–30 mg of the native tissue and the decellularized matrices obtained by the different protocols (n = 3).

massive Alciane blue staining was detected after processing the tissue with protocol 5. That observation suggested that fat extraction with hexane and acetone followed by nuclease treatment and mild detergents and hypertonic treatments has led to less damage to the GAGs than the other cell extracting steps such as trypsin digestion, continuous agitation in detergents, or freezing and thawing. However, these processes resulted in more efficient cell removal. Overall we have noticed that the GAGs were better preserved by the processes that did not involve trypsin digestion (i.e. protocols 3–5). We have noticed that cell removal and lipid extraction steps condensed the decellularized tissues. Therefore, the processed tissues exhibited stronger staining as compared to the native omentum.

We next sought to quantify the remaining sulfated GAGs (figure 4(B)). Using Blyscan assay we have found that prior to decellularization the native tissue contained 0.59 μg ± 0.13 sulfated GAGs per mg dry tissue. As a result of the decellularization and fat extraction, the ECM content per mg tissue has increased. Consequently, the content of the sulfated GAGs in the processed tissues was higher than in the native tissue. Figure 4(B) revealed the amount of sulfated GAGs per mg after processing by protocols 1–5. The amount of sulfated GAGs per mg dry tissue in the matrix obtained by protocol 3 was significantly lower than in the matrix obtained by protocol 4 due to the high lipid content, which diluted other ECM components. The sulfated GAG contents in protocols 4 and 5 were significantly higher than in protocols 1 and 2. Overall, these results may suggest that the combination of detergents and tonicity is less destructive for GAGs in the ECM as compared to trypsin digestion and freezing and thawing.

Matrix morphology

The internal morphology of the matrix can dictate the growth and assembly of the engineered tissue [37]. Therefore, we

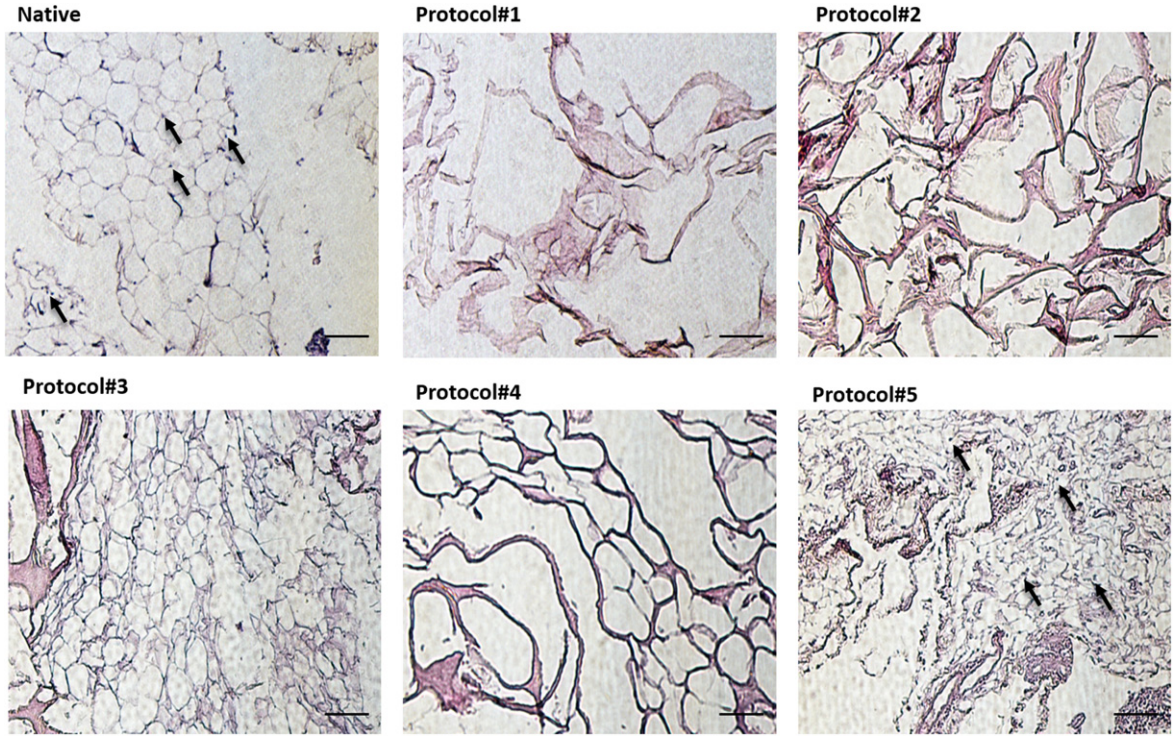

Figure 3. Cell removal. H&E stained sections of the native tissue and the decellularized matrices obtained by the different protocols. Nuclei stained blue (indicated by arrows), cytoplasm and extracellular proteins stained pink (scale bar = 100 μm).

next sought to evaluate the morphology of the matrices by SEM.

As shown in figure 5, the different decellularization processes resulted in a distinct matrix morphology. The matrix obtained by protocol 1 had on average a relatively small fiber diameter (1.1 μm ± 0.087) and the mean pore area of that matrix was significantly the largest (975.6 μm^2 ± 112.5, $P < 0.05$). While protocols 2–4 resulted in an average fiber diameter at the same range, protocol 5 resulted in significantly higher diameter fibers (2.464 μm ± 0.104; $P < 0.0005$). Since not all cell components were efficiently removed by protocol 5, the obtained pores were smaller (389.6 μm^2 ± 41.63). Protocols 2 and 3 have yielded matrices with two regions, similar to the native tissue. Due to the poor fat removal, the fatty area was covered with lipids and therefore was not porous; however the translucent area was more fibrous and therefore had more open space. Overall the mean pore area of the matrices obtained by protocols 2 and 3 were relatively small (184.3 μm^2 ± 22.14 and 260.3 μm^2 ± 68.6, $P < 0.05$ respectively). The matrix obtained by protocol 4 had a pore area of 619.1 μm^2 ± 107.2, significantly higher than the pore area obtained by protocols 2 and 3. Overall, the average pore size was significantly smaller than the values obtained with protocol 1.

Recent studies have shown that the fiber diameter and the pore area of the scaffolds may affect cells attachment, infiltration and even differentiation or proliferation [38–41]. All the decellularized matrices exhibited a fiber diameter of about 1–2 μm, similar to that of collagen fibers that are abundant in the ECM of the omentum [38, 42, 43]. Therefore we assumed that all cells that are surrounded by collagen in their natural niche, such as fibroblasts, cardiomyocytes, mesenchymal stem cells etc, will benefit from those scaffold fibers. Furthermore some studies have revealed that large pore areas (larger than 350 μm^2) are more suitable for cell infiltration and adhesion [40, 41]. Protocols 1, 4 and 5 have resulted in scaffolds with large pores and therefore are assumed to be more appropriate for tissue engineering.

Cell adhesion and viability

Cell–matrix interactions are essential for engineering homogenous tissues. We next sought to evaluate the ability of cells to adhere to the different scaffolds. NIH 3T3 cells were mixed with a culture medium and seeded on the scaffolds with a single droplet. Three hours post-seeding (defined as day 0) the cell constructs were washed carefully and the existence of viable cells in the scaffolds was assessed using an XTT metabolic assay. As shown in figure 6, a significantly higher number of viable cells was detected within the scaffolds obtained by protocol 1 as compared to scaffolds obtained by all other protocols. A neglectable number of viable cells was detected in scaffolds obtained by protocol 5. This may be attributed to the inefficient decellularization process and the existence of toxic cellular materials that remained within the scaffold.

We next evaluated the proliferation of EGFP expressing fibroblasts in the different scaffolds. Figure 7(A) shows fluorescence images of fibroblasts in the different scaffolds on day 2 (upper panel) and day 8 (lower panel). As shown, higher cell concentrations were observed in the scaffolds obtained by protocols 1, 2 and 4, as compared to scaffolds

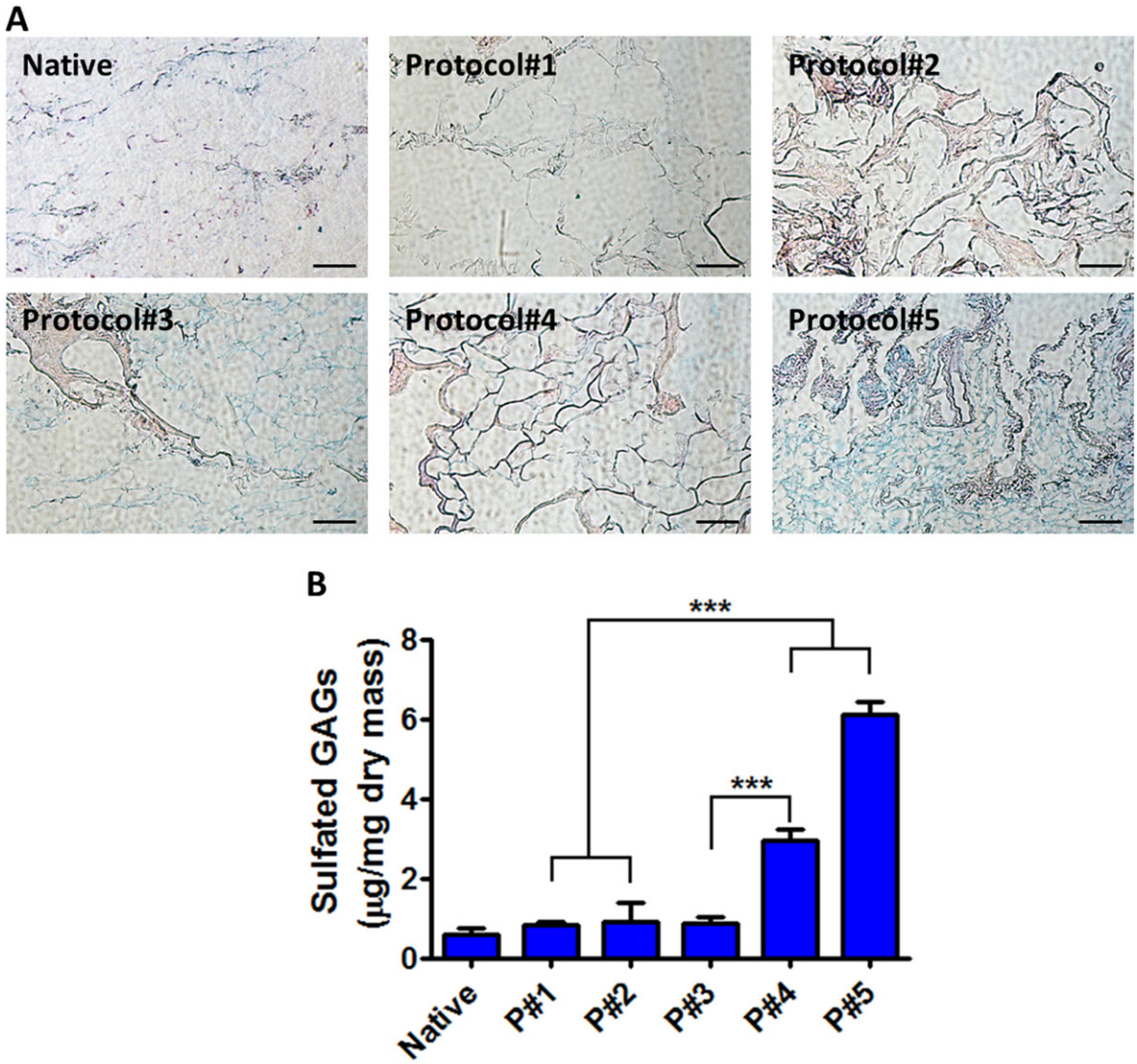

Figure 4. Glycosaminoglycan (GAG) content. A: Alcian blue and fast red stained sections of the native tissue and the decellularized matrices obtained by the different protocols. GAGs stained light blue, nuclei stained red and proteins stained pale pink (scale bar = 100 μm). B: Measurement of sulfated GAGs in the decellularized matrices obtained by the different protocols. Results are presented as mean μg sulfated GAGs per mg dry mass (n = 4).

prepared by protocols 3 and 5. To quantify cell growth over the culture period we used an XTT assay. We noticed a significant increase by day 8 in the average O.D at 450 nm in scaffolds obtained by protocols 1, 2 and 4, while a limited expansion rate was observed in scaffolds obtained by protocols 3 and 5 (figure 7(B)). Although a similar O.D was observed at day 8 in protocols 1, 2 and 4, considering the initial low number of attached cells in protocol 4, the proliferation rate in these scaffolds was higher than that of scaffolds obtained by protocols 1 and 2. Similarly, the limited proliferation rate observed in scaffolds obtained by protocol 5 may be attributed to the initial lower cell attachment. Therefore we concluded that scaffolds obtained by protocol 5 are not appropriate for tissue engineering. We believe that the high water absorbance of scaffolds obtained by protocol 1 is related to the high capacity of cell attachment. We further state that due to the high adhesion that has been observed, these scaffolds may be suitable for culturing cells with a limited or nonexistent proliferation potential, such as cardiomyocytes.

Cell organization and tissue assembly

The omentum is highly vascularized and its fibrillar ECM is rich with collagens, adhesive proteins and GAGs [44]. Furthermore the omentum has regenerative properties [9, 13]. Taken together, these properties have previously led us to explore the potential of the omental matrix to support cardiac tissue assembly [22]. We next sought to assess the potential of the decellularized matrices to serve as scaffolds directing functional assembly of cardiac tissues. Recently, it was shown that various topographies within the scaffold may affect cardiac cell behavior and tissue organization in a distinct manner [6]. Therefore, we hypothesized that the diverse morphologies of the scaffolds, including pore area and fiber diameter, may

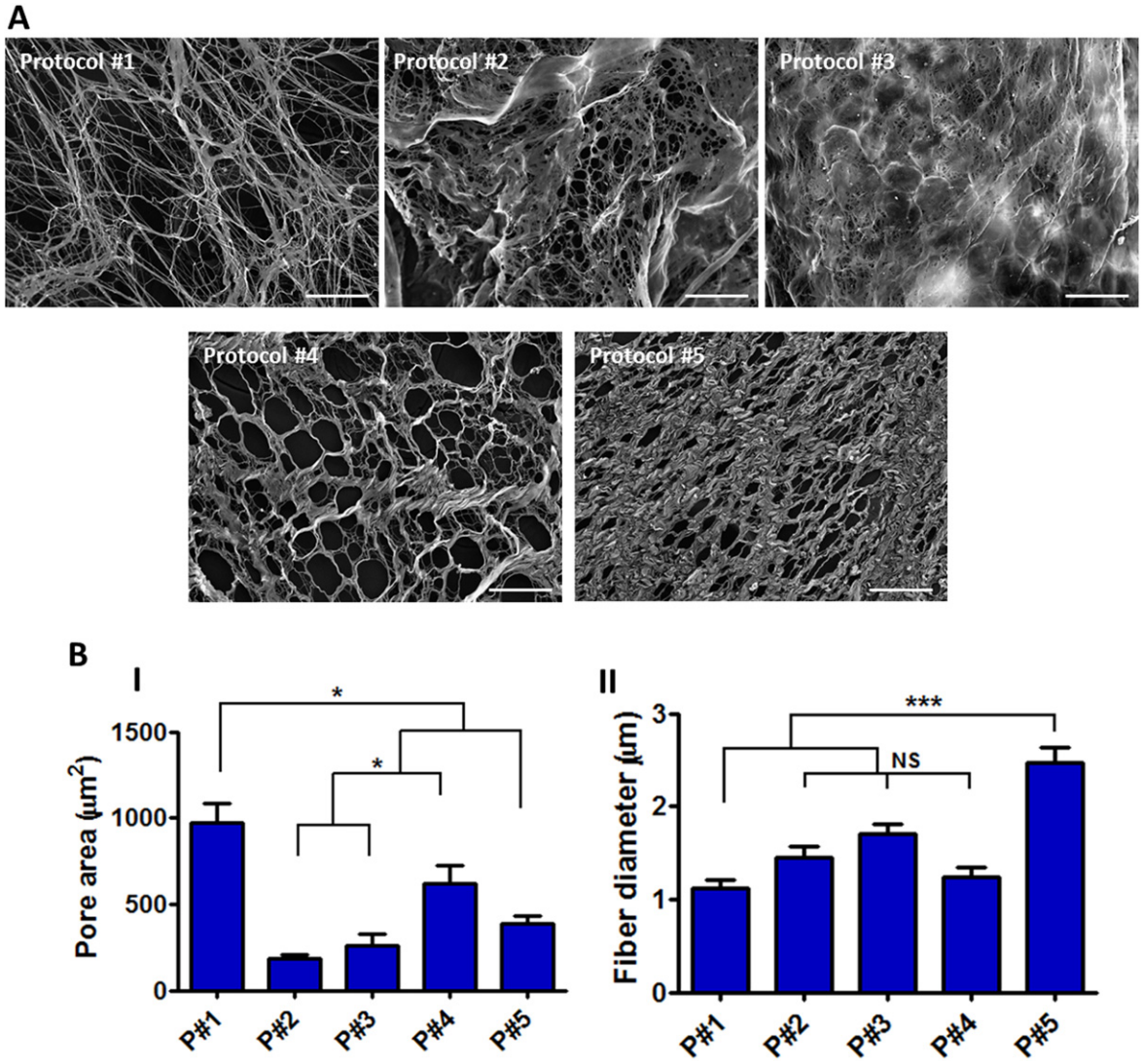

Figure 5. Matrix morphology. A: Representative SEM images of the matrices obtained by the different protocols (scale bar = 100 μm). B: Measurements of the structural properties of the different matrices as observed in the SEM images: (I) mean pore area in μm^2, (II) mean fiber diameter in μm.

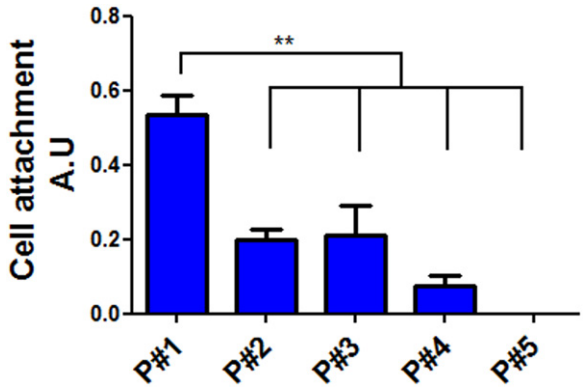

Figure 6. Cell attachment to the scaffolds. NIH-3T3 cells (10^5) were seeded on the scaffolds obtained by the different protocols. Cell attachment to the scaffolds was measured by the O.D of the XTT assay 3 h after seeding. Results are represented as the mean delta between the optical densities (O.D) at 450 nm and at 630 nm (n = 3).

result in distinct cell morphologies. In cardiac tissue engineering, an optimal scaffolding material should promote elongation and alignment of the cultured cells, and direct their organization into functional cardiac patches generating strong contraction forces [45]. To assess cardiac cell organization within the scaffolds, cells were isolated from ventricles of neonatal rats and seeded on the different matrices as we previously described [22]. Immunostaining of cardiomyocytes with antibodies against sarcomeric actinin revealed distinct morphologies within the different scaffolds. While decellularization protocols 3–5 resulted in rounded cells with limited actinin striation, cells seeded within scaffolds obtained by protocols 1 and 2 showed an elongated morphology. Furthermore, massive and organized actinin expression was observed in these cultures. Analysis for cardiomyocyte elongation revealed a significantly higher aspect ratio in cells cultured on matrices obtained by protocol 1 and 2 as compared to matrices obtained by protocols 3–5 (figure 8(B)). A higher aspect ratio may lead to anisotropic

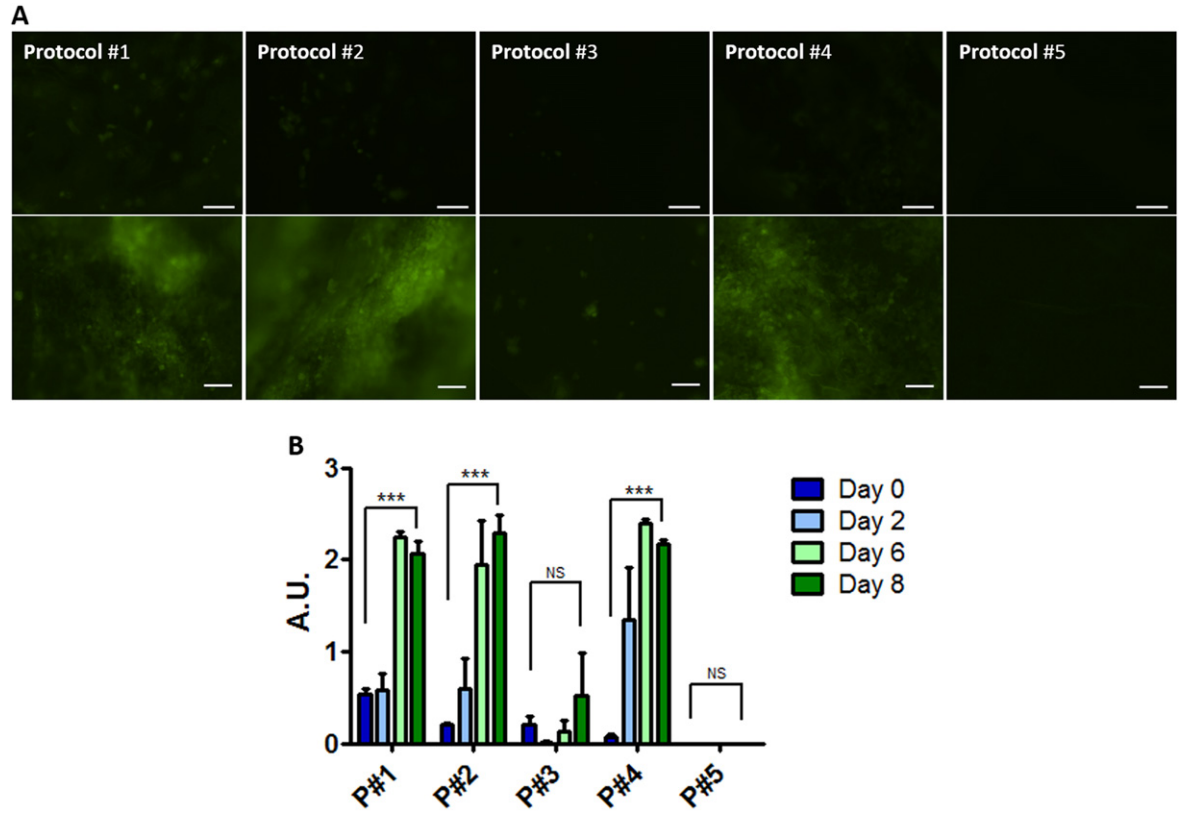

Figure 7. Cell proliferation on the scaffolds. A: Fluorescent images of EGFP expressing NIH-3T3 cells on the scaffolds obtained by the different protocols after 2 (top) or 8 (Bottom) days culture (scale bar = 100 μm). B: XTT metabolic activity assay. Results are represented as the mean delta between the optical densities (O.D) at 450 nm and at 630 nm (n = 3).

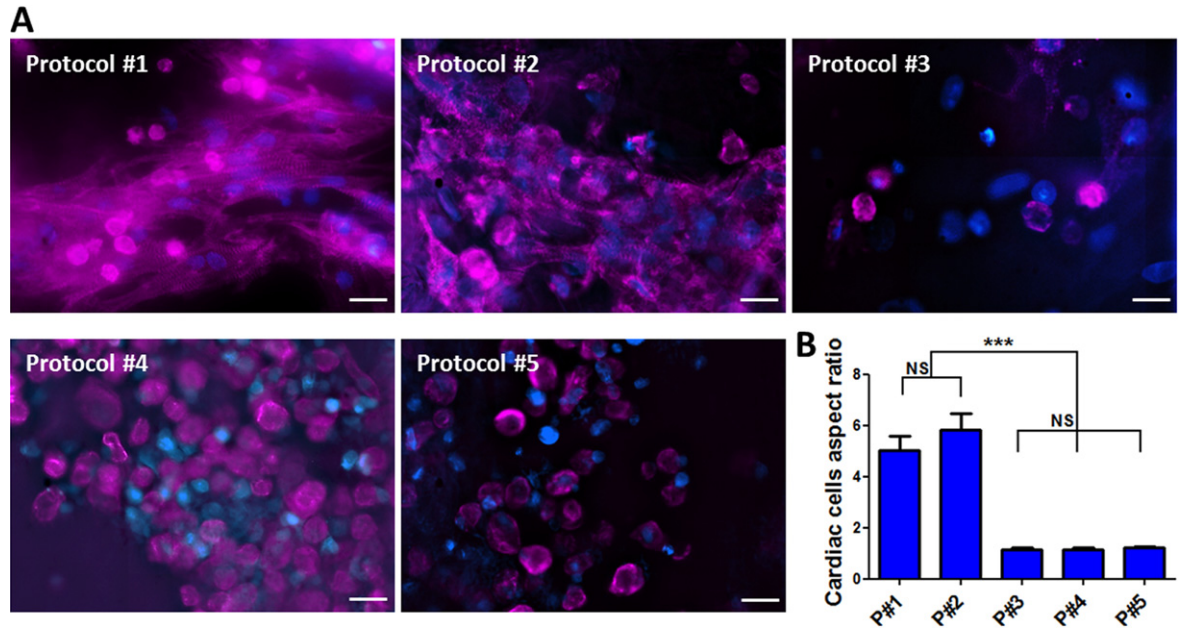

Figure 8. Cardiomyocytes organization within the scaffolds. A: Bar = 10 μm. Fluorescent images of stained cardiomyocytes on the scaffolds obtained by the different protocols. Nuclei stained blue and actinin stained pink. B: Cardiomyocyte aspect ratio.

contraction of cardiac patches [7, 46, 47]. In contrast to our initial assumption, the topographies of the scaffolds that were processed by protocols 1 and 2 are significantly different (figure 5). Since cardiomyocytes acquired a natural appearance on both scaffolds, we assumed that the cardiomyocyte organization depended on other parameters, such as water absorbance or biochemical content.

Conclusions

A decellularized matrix of the omentum has the potential to serve as a scaffold for the engineering of various tissues, as recently reported [22].

Here, we have optimized the decellularization process assessing cell removal efficiency, biochemical content and matrix morphology. We have also evaluated the effect of the different parameters on seeded cells' viability and proliferation, and on the assembly of cardiac tissues. We have shown that several of the investigated decellularization protocols were not efficient. For example the use of acetone for fat removal is not sufficient by itself (protocol 3), and a short exposure to hypertonic tension and mild detergents for cell removal is not efficient (protocol 5). We have concluded that aggressive processing of the omentum, such as trypsin digestion, freezing and thawing resulted in a complete acellular matrix that is compatible for cell culture and tissue assembly. Nevertheless, the tissues that were processed by milder conditions such as detergents and osmotic pressure resulted in scaffolds that better resemble the native tissue, indicating that many ECM components were intact. Furthermore, we have deduced that all lipids must be extracted from the tissue in order to induce cell attachment, maintain cell viability and promote proper assembly of cells to tissues.

Although the decellularized matrix technology is already in clinical settings, several studies reported on massive inflammation, pain and graft rejection after transplantation [32, 48–50]. A possible advantage of using decellularized omentum as a scaffold for tissue engineering is the potential autologous source of the matrix. Contrary to the widely used xenogeneic matrices, the omentum can be easily and safely harvested from the same patient and quickly manipulated to obtain perhaps a more biocompatible scaffold [23, 27]. Such a matrix, combined with the patient's own cells, has the potential to represent a new concept of engineering completely autologous tissues (figure 9) [22]. This unique approach may allow, for the first time, to engineer a completely personalized tissue comprised of the patient's own cells and matrix.

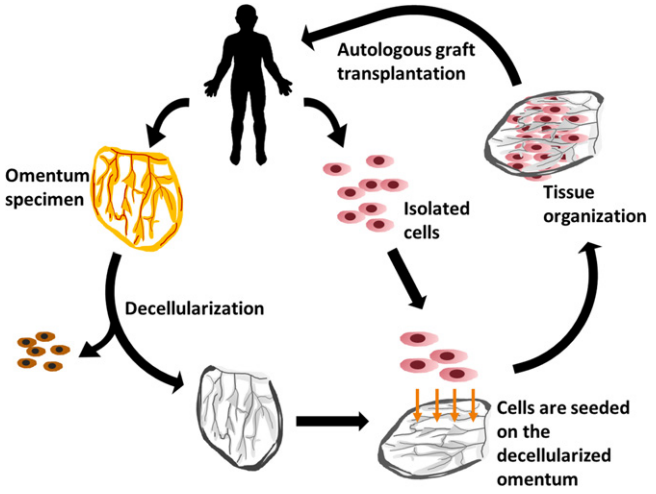

Figure 9. Schematic illustration of the potential of the decellularized omentum approach for autologous tissue engineering. A specimen from the omentum is harvested from the patient. Following this, all cells and lipids are extracted from the omentum by decellularization methods. Isolated cells from the same patient are seeded on the decellularized scaffold and constitute a functional tissue. The engineered tissue can be implanted in the patient with a low risk of rejection.

Acknowledgment

T.D acknowledges support from the European Union FP7 program (Marie Curie, CIG), Alon Fellowship, Israel Science Foundation and the Nicholas and Elizabeth Slezak Super Center for Cardiac Research and Biomedical Engineering at Tel Aviv University. The work is part of the doctoral thesis of N.S.T. at Tel-Aviv University.

References

[1] Schwindt R and Vining A R 1986 Proposal for a future delivery market for transplant organs *Journal of Health Politics, Policy and Law* **11** 483–500

[2] Fentiman L C 1994 Organ donations: the failure of altruism *Issues in Science and Technology* **11** 43–8 www.ncbi.nlm.nih.gov/pubmed/10154971

[3] Anonymous 2012 *Organ Procurement and Transplantation Network (OPTN) and Scientific Registry of Transplant Recipients (SRTR)* Annual Data Report http://srtr.transplant.hrsa.gov/annual_reports/2011/pdf/2011_SRTR_ADR.pdf

[4] Burk J, Badylak S F, Kelly J and Brehm W 2013 Equine cellular therapy–from stall to bench to bedside? *Cytometry. Part A: The Journal of the International Society for Analytical Cytology* **83** 103–13 www.ncbi.nlm.nih.gov/pubmed/23081833

[5] Vunjak-Novakovic G *et al* 2010 Challenges in cardiac tissue engineering *Tissue Eng. Part B, Reviews* **16** 169–87

[6] Fleischer S and Dvir T 2013 Tissue engineering on the nanoscale: lessons from the heart *Current Opinion in Biotechnology* **24** 664–71

[7] Dvir T, Timko B P, Kohane D S and Langer R 2011 Nanotechnological strategies for engineering complex tissues *Nat. Nanotechnology* **6** 13–22

[8] Yang S, Leong K F, Du Z and Chua C K 2001 The design of scaffolds for use in tissue engineering. Part I. Traditional factors *Tissue Eng.* **7** 679–89

[9] Tsang K Y, Cheung M C, Chan D and Cheah K S 2010 The developmental roles of the extracellular matrix: beyond structure to regulation *Cell Tissue Res.* **339** 93–110

[10] Comoglio P M, Boccaccio C and Trusolino L 2003 Interactions between growth factor receptors and adhesion molecules: breaking the rules *Current Opinion in Cell Biology* **15** 565–71

[11] Giancotti F G and Ruoslahti E 1999 Integrin signaling *Science* **285** 1028–32

[12] Lindahl U and Hook M 1978 Glycosaminoglycans and their binding to biological macromolecules *Ann. Rev. Biochem.* **47** 385–417

[13] Hoshiba T, Lu H, Kawazoe N and Chen G 2010 Decellularized matrices for tissue engineering *Expert Opinion on Biological Therapy* **10** 1717–28

[14] Manabe R *et al* 2008 Transcriptome-based systematic identification of extracellular matrix proteins *Proc. Natl. Acad. Sci. USA* **105** 12849–54

[15] Badylak S F 2007 The extracellular matrix as a biologic scaffold material *Biomaterials* **28** 3587–93
[16] Ott H C *et al* 2008 Perfusion-decellularized matrix: using nature's platform to engineer a bioartificial heart *Nat. Med.* **14** 213–21
[17] Flynn L E 2010 The use of decellularized adipose tissue to provide an inductive microenvironment for the adipogenic differentiation of human adipose-derived stem cells *Biomaterials* **31** 4715–24
[18] Dahms S E, Piechota H J, Dahiya R, Lue T F and Tanagho E A 1998 Composition and biomechanical properties of the bladder acellular matrix graft: comparative analysis in rat, pig and human *British Journal of Urology* **82** 411–9
[19] Schenke-Layland K *et al* 2003 Impact of decellularization of xenogeneic tissue on extracellular matrix integrity for tissue engineering of heart valves *J. Struct. Biol.* **143** 201–8
[20] Valentin J E, Badylak J S, McCabe G P and Badylak S F 2006 Extracellular matrix bioscaffolds for orthopaedic applications. A comparative histologic study *The Journal of Bone and Joint Surgery. American volume* **88** 2673–86
[21] Gilbert T W, Sellaro T L and Badylak S F 2006 Decellularization of tissues and organs *Biomaterials* **27** 3675–83 www.ncbi.nlm.nih.gov/pubmed/16519932
[22] Shevach M, Soffer-Tsur N, Fleischer S, Shapira A and Dvir T 2014 Fabrication of omentum-based matrix for engineering vascularized cardiac tissues *Biofabrication* **6** 024101 www.ncbi.nlm.nih.gov/pubmed/24464690
[23] Collins D, Hogan A M, O'Shea D and Winter D C 2009 The omentum: anatomical, metabolic, and surgical aspects *Journal of Gastrointestinal Surgery: Official Journal of the Society for Surgery of the Alimentary Tract* **13** 1138–46
[24] Patel R S *et al* 2009 Morbidity and functional outcomes following gastro-omental free flap reconstruction of circumferential pharyngeal defects *Head & Neck* **31** 655–63
[25] Shelton E L, Poole S D, Reese J and Bader D M 2013 Omental grafting: a cell-based therapy for blood vessel repair *J. Tissue Eng. Regen. Med.* **7** 421–33
[26] Dvir T, Levy O, Shachar M, Granot Y and Cohen S 2007 Activation of the ERK1/2 cascade via pulsatile interstitial fluid flow promotes cardiac tissue assembly *Tissue Eng.* **13** 2185–93
[27] Liebermann-Meffert D 2000 The greater omentum. Anatomy, embryology, and surgical applications *The Surgical Clinics of North America* **80** 275–93 xii
[28] Hayat M A 2012 *Stem Cells and Cancer Stem Cells: Therapeutic Applications in Disease and Injury* vol 9 (New York: Springer)
[29] Brown B N *et al* 2011 Comparison of three methods for the derivation of a biologic scaffold composed of adipose tissue extracellular matrix *Tissue Eng. Part C, Methods* **17** 411–21
[30] Zahler P and Niggli V 1977 The use of organic solvents in membrane research *Methods in Membrane Biology* **8** 1–50 http://link.springer.com/chapter/10.1007%2F978-1-4684-2910-7_1
[31] Christie W W 1993 *Advances in Lipid Methodology* (Dundee: Oily Press) pp 195–213 http://lipidlibrary.aocs.org/topics/extract2/file.pdf
[32] Badylak S F, Freytes D O and Gilbert T W 2009 Extracellular matrix as a biological scaffold material: structure and function *Acta Biomaterialia* **5** 1–13
[33] Yang C *et al* 2009 Patent EP 2229191 www.lens.org/lens/patent/EP_2229191_B1
[34] Porzionato A *et al* 2013 Decellularized omentum as novel biologic scaffold for reconstructive surgery and regenerative medicine *Eur. J. Histochem.: EJH* **57** e4 www.ncbi.nlm.nih.gov/pubmed/23549463
[35] Crapo P M, Gilbert T W and Badylak S F 2011 An overview of tissue and whole organ decellularization processes *Biomaterials* **32** 3233–43
[36] Linhardt R J and Toida T 2004 Role of glycosaminoglycans in cellular communication *Acc. Chem. Res.* **37** 431–8
[37] Bettinger C J, Langer R and Borenstein J T 2009 Engineering substrate topography at the micro- and nanoscale to control cell function *Angew Chem Int Ed Engl* **48** 5406–15
[38] Erisken C, Zhang X, Moffat K L, Levine W N and Lu H H 2013 Scaffold fiber diameter regulates human tendon fibroblast growth and differentiation *Tissue Eng. Part* A **19** 519–28
[39] Balguid A *et al* 2009 Tailoring fiber diameter in electrospun poly(epsilon-caprolactone) scaffolds for optimal cellular infiltration in cardiovascular tissue engineering *Tissue Eng. Part* A **15** 437–44
[40] Murphy C M, Haugh M G and O'Brien F J 2010 The effect of mean pore size on cell attachment, proliferation and migration in collagen-glycosaminoglycan scaffolds for bone tissue engineering *Biomaterials* **31** 461–6
[41] O'Brien F J *et al* 2007 The effect of pore size on permeability and cell attachment in collagen scaffolds for tissue engineering *Technology and Health Care: Official Journal of the European Society for Engineering and Medicine* **15** 3–17 www.ncbi.nlm.nih.gov/pubmed/17264409
[42] Litbarg N O *et al* 2007 Activated omentum becomes rich in factors that promote healing and tissue regeneration *Cell Tissue Res.* **328** 487–97
[43] Hishida M *et al* 2010 Omental flap closure of refractory wounds: rat model *Nagoya Journal of Medical Science* **72** 91–9 www.ncbi.nlm.nih.gov/pubmed/20229707
[44] Platell C, Cooper D, Papadimitriou J M and Hall J C 2000 The omentum *World J. Gastroenterol.: WJG* **6** 169–76 www.ncbi.nlm.nih.gov/pubmed/11819552
[45] Iyer R K, Chiu L L, Reis L A and Radisic M 2011 Engineered cardiac tissues *Current Opinion in Biotechnology* **22** 706–14
[46] Shevach M, Maoz B M, Feiner R, Shapira A and Dvir T 2013 Nanoengineering gold particle composite fibers for cardiac tissue engineering *J. Mater. Chem.* B **1** 5210–7
[47] Fleischer S *et al* 2014 Albumin fiber scaffolds for engineering functional cardiac tissues *Biotechnol. Bioeng.* **111** 1246–57 www.ncbi.nlm.nih.gov/pubmed/24420414
[48] Badylak S F, Taylor D and Uygun K 2011 Whole-organ tissue engineering: decellularization and recellularization of three-dimensional matrix scaffolds *Ann. Rev. Biomed. Eng.* **13** 27–53
[49] Cissell D D, Hu J C, Griffiths L G and Athanasiou K A 2014 Antigen removal for the production of biomechanically functional, xenogeneic tissue grafts *J. Biomech.* **47** 1987–96 www.ncbi.nlm.nih.gov/pubmed/24268315
[50] Fishman J M *et al* 2013 Immunomodulatory effect of a decellularized skeletal muscle scaffold in a discordant xenotransplantation model *Proc. Natl. Acad. Sci. USA* **110** 14360–5